# GEM reconnection challenge: Implicit kinetic simulations with the physical mass ratio

Paolo Ricci,[1,2] Giovanni Lapenta,[1,3] and J. U. Brackbill[3]

Received 11 April 2002; revised 31 May 2002; accepted 20 June 2002; published 3 December 2002.

[1] We extend kinetic simulations of the Geospace Environment Modeling (GEM) magnetic reconnection challenge [Birn et al., *J. Geophys. Res.*, 106, 3715, 2001] to a physical mass ratio, using the implicit Particle-in-Cell (PIC) code CELESTE3D which allows the use of a coarser grid and a bigger time step. We compare results for three values of the mass ratio $m_i/m_e = 25$ (GEM challenge standard mass ratio), $m_i/m_e = 180$ and the physical mass ratio $m_i/m_e = 1836$. The results of the three simulations are compared and the scaling laws based on reconnection via nongyrotropic electron pressure are verified. *INDEX TERMS:* 7835 Space Plasma Physics: Magnetic reconnection; 7843 Space Plasma Physics: Numerical simulation studies; 2764 Magnetospheric Physics: Plasma sheet; 7839 Space Plasma Physics: Nonlinear phenomena. **Citation:** Ricci, P., G. Lapenta, and J. U. Brackbill, GEM reconnection challenge: Implicit kinetic simulations with the physical mass ratio, *Geophys. Res. Lett.*, *29*(23), 2088, doi:10.1029/2002GL015314, 2002.

## 1. Introduction

[2] The Geospace Environment Modeling (GEM) magnetic reconnection challenge [*Birn et al.*, 2001] seeks to understand the physics of fast magnetic reconnection in the magnetotail [*Oieroset et al.*, 2001] by investigating a standard 2-dimensional configuration based on a Harris current sheet. Different models are compared: Resistive magnetohydrodynamics (MHD), Hall MHD, hybrid, and full particle (kinetic) codes [*Birn et al.*, 2001, and references therein]. The standard configuration assumes a mass ratio $m_i/m_e = 25$. Kinetic simulations with mass ratios up to 100 are described [*Hesse et al.*, 1999; *Pritchett*, 2001a; *Shay et al.*, 2001].

[3] We extend the simulations to mass ratios $m_i/m_e = 180$ and $m_i/m_e = 1836$. The results show that large scale phenomena, such as the reconnection rate, are not affected by the mass ratio, but that the electron behavior in the dissipation region is affected. The findings of previous simulations at low mass ratios are recovered, and the use of the physical mass ratio allows a comparison of the predictions of the scaling laws over a broader mass ratio range, and a better discrimination between the scaling laws based on nongyrotropic electron pressure [*Laval et al.*, 1966; *Hesse et al.*, 1999; *Kuznetsova et al.*, 2000] and scaling laws based on electron inertia [*Burkhart et al.*, 1990]. In particular, the scaling with mass ratio based on reconnection via nongyrotropic electron pressure is recovered.

## 2. Initial Conditions and the Simulation Approach

[4] We consider a Harris current sheet in the $(x, z)$ plane [*Birn et al.*, 2001], with magnetic field given by $B_{0x}(z) = B_0 \tanh(z/\lambda)$ and density by $n_0(z) = n_0\ \mathrm{sech}^2\ (z/\lambda) + n_b$.

[5] The system size is $L_x \times L_z = 25.6\ c/\omega_{pi} \times 12.8\ c/\omega_{pi}$, where the ion inertial length, $c/\omega_{pi}$, is defined using the density $n_0$. The temperature ratio is $T_e/T_i = 0.2$, the current sheet thickness is $\lambda = 0.5c/\omega_{pi}$, the background density is $n_b = 0.2\ n_0$, the ion drift velocity in the $y$ direction is $V_{i0} = 1.67V_A$, where $V_A$ is the Alfvén velocity, and $V_{e0}/V_{i0} = -T_{e0}/T_{i0}$. The initial perturbation is specified by a perturbed potential vector $A_y$ of the form

$$A_y = -A_{y0} \cos(2\pi x/L_x) \cos(\pi z/L_z) \quad (1)$$

with $A_{y0} = 0.1\ B_0 c/\omega_{pi}$. We use the implicit Particle-in-Cell (PIC) code CELESTE3D to solve the full set of Maxwell-Vlasov equations [*Brackbill and Forslund*, 1985; *Vu and Brackbill*, 1992; *Ricci et al.*, 2002]. Implicit moment PIC allows more rapid simulations on ion length and time scales than explicit methods, while retaining the kinetic effects of both the electrons and ions. The explicit simulation time step limit, $\Delta t < 2/\omega_{pe}$, and the mesh spacing required to avoid the finite grid instability, $\Delta x/\lambda_{De} < 1$, where $\lambda_{De}$ is the electron Debye length, are replaced in implicit simulations by an accuracy condition, $v_{th,e}\ \Delta t < \Delta x$, whose principal effect is to determine how well energy is conserved.

[6] The cost of an explicit simulation on ion scales varies with the ion to electron mass ratio as $(m_i/m_e)^{(d+2)/2}$, where $d$ is the number of spatial dimensions [*Pritchett*, 2000]. For example, for the GEM challenge, an explicit simulation with $m_i/m_e = 1836$ is more than 5000 times as expensive as one with $m_i/m_e = 25$. In contrast, the cost of an implicit simulation scales as $(m_i/m_e)^{1/2}$, as the time step can be kept constant with respect to the ion plasma frequency and the ratio $\omega_{ci}/\omega_{pi}$ scales as $(m_i/m_e)^{1/2}$ to maintain the same Harris current sheet equilibrium. However, for the results shown here, the time step is reduced from $\omega_{pi}\ \Delta t = 0.3$ for $m_i/m_e = 25$ to $\omega_{pi}\ \Delta t = 0.05$ for $m_i/m_e = 1836$, with which excellent energy conservation is obtained.

[7] With $m_i/m_e = 25$, the GEM challenge is simulated with CELESTE3D on a $N_x \times N_z = 64 \times 64$ grid, with time step $\omega_{pi}\ \Delta t = 0.3$, and 25 particles per species per cell, for a total of $2 \cdot 10^5$ computational particles. For comparison, the explicit PIC simulation presented by Pritchett [*Pritchett*, 2001a] employs a $N_x \times N_z = 512 \times 256$ grid, $9.12 \cdot 10^6$ computational particles and a time step $\omega_{pe}\Delta t = 0.15$,

[1]Istituto Nazionale per la Fisica della Materia (INFM), Dipartimento di Fisica, Politecnico di Torino, Torino, Italy.
[2]Dipartimento di Energetica, Politecnico di Torino, Torino, Italy.
[3]Theoretical Division, Los Alamos National Laboratory, Los Alamos, New Mexico, USA.


0094-8276/02/2002GL015314

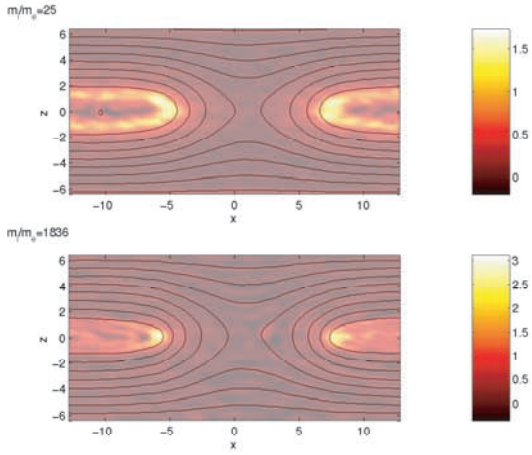


**Figure 1.** Magnetic field lines and out-of-plane current density (color coded, normalized to $en_0V_A$) are shown at $\omega_{ci}t = 40$ for $m_i/m_e = 25$ (top) and $m_i/m_e = 1836$ (bottom).

corresponding to $\omega_{pi}\,\Delta t = 0.03$ (i.e., 10 times smaller than ours). Results with CELESTE3D are comparable in detail with those of explicit simulations for $m_i/m_e = 25$ [*Ricci et al.*, 2002].

[8] Certainly, the accuracy of wave-particle interactions on the electron time scale is less using a coarser grid and a bigger time step. However, results of many simulations show that kinetic electrons correctly contribute inertial effects, anisotropic pressure and electron thermal transport on ion time and length scales [*Forslund and Brackbill*, 1982; *Brackbill et al.*, 1984; *Lapenta and Brackbill*, 1996; *Vu and Brackbill*, 1993]. In particular, for the GEM challenge simulation in the case of realistic mass ratio, both the electron inertia length and the electron diffusion region in the $z$ direction are not resolved. However, the important physical spatial scales appear to be present and described correctly, as a comparison with the scaling laws shows.

## 3. Reconnection Rate

[9] The GEM reconection challenge has been performed with mass ratios $m_i/m_e = 25$, 180, and 1836. Distances are normalized to $c/\omega_{pi}$, velocities to $V_A$, the magnetic field to $B_0$, and the density to $n_0$.

[10] Figure 1 shows the out-of-plane current density and magnetic field lines at $\omega_{ci}t = 40$ for $m_i/m_e = 25$ and $m_i/m_e = 1836$. The out-of-plane current has evolved, starting from an initially uniform current sheet. For both mass ratios, a saddle point at the X point is created. The evolution of the magnetic field lines which form an X point in the center of the domain reveals that at the highest mass ratio reconnection proceeds slightly further, the current is more filamentary, and the maximum current density is twice as large.

[11] To evaluate the reconnection rate, the flux difference between the X and the O points, $\Delta\,\Psi$, is used. Figure 2 shows the evolution of the reconnected flux for the different mass ratios. A slow initial growth, which lasts roughly until $\omega_{ci}t \approx 10$, is succeeded by more rapid growth until $\omega_{ci}t \approx 25$, at similar values of the reconnected flux in all cases. The reconnection rate increases slightly from the lowest to the highest mass ratio, but not monotonically. This fact points out that the electron mass appears to have only a small

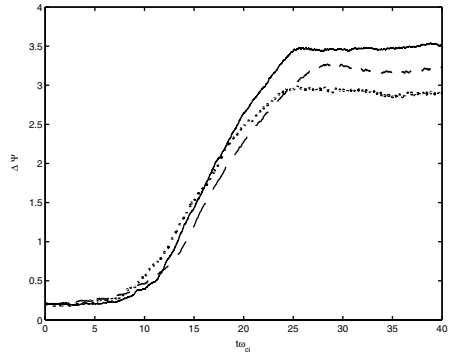


**Figure 2.** The reconnected flux (normalized to $B_0c/\omega_{pi}$) is shown for $m_i/m_e = 25$ (dashed line), $m_i/m_e = 180$ (dotted line), and $m_i/m_e = 1836$ (solid line).

effect on the the large scale evolution. "The electron physics in the dissipation region adjusts itself to accommodate the large scale evolution... (which) should be controlled by the inertia of ions... independent of the local electron physics" [p. 1785, *Hesse et al.*, 1999].

[12] In the two dimensional configuration we are considering, the reconnection is driven by the $y$ component of the electric field **E** at the X point, $E_{y,rec}$, and it is [*Pritchett*, 2001a]

$$E_{y,rec} = -\frac{1}{c}\left(v_{ze}B_x - v_{xe}B_z\right) - \frac{1}{en_e}\left(\frac{\partial P_{xye}}{\partial x} + \frac{\partial P_{yze}}{\partial z}\right) - \frac{m_e}{e}\left(\frac{\partial v_{ye}}{\partial t} + v_{xe}\frac{\partial v_{ye}}{\partial x} + v_{ze}\frac{\partial v_{ye}}{\partial z}\right) \quad (2)$$

[13] Our simulations support the idea that the nongyrotropic electron pressure contributions to $E_{y,rec}$ are important [*Hesse et al.*, 1999; *Hesse et al.*, 2001; *Kuznetsova et al.*, 2001; *Pritchett*, 2001a], as they account for approximately 70% of $E_{y,rec}$ at the reconnection site, Figure 3, for $m_i/m_e = 180$.

## 4. The Diffusion Region

[14] The large scale behavior of the simulations is shown in Figure 4, extending to the realistic mass ratio the

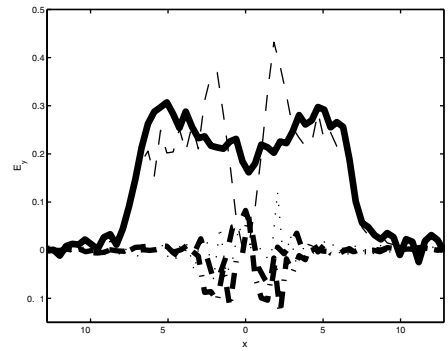


**Figure 3.** Out-of-plane electric field, $E_y$ (thick solid), for $m_i/m_e = 180$, $z = 0$, $t\omega_{ci} = 15$ and its contributions: $-1/(en_e)\ \partial P_{xye}/\partial x$ (thick dashed), $-1/(en_e)\ \partial P_{zye}/\partial z$ (thick dash-dotted), $v_{xe}B_z/c$ (dashed), $-m_e/e \cdot v_{xe}\partial v_{ey}/\partial x$ (dotted).

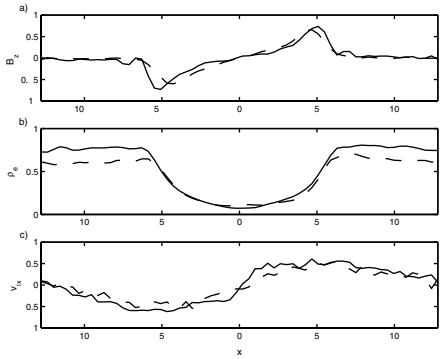

**Figure 4.** $z$-component of the magnetic field, $B_z$, (a); electron density, $\rho_e$, (b); $x$-component of the ion velocity, $v_{xi}$, (c) for $z = 0$, at $\omega_{ci}t = 15$ and for $m_i/m_e = 25$ (dashed line) and $m_i/m_e = 1836$ (solid line).

considerations by *Hesse et al.* [1999]. Comparing the simulations with $m_i/m_e = 25$ and $m_i/m_e = 1836$, the $z$-component of the magnetic field, the $x$-component of the ion velocity and the electron density are displayed for $z = 0$ and $\omega_{ci}t = 15$. Despite some small differences (the derivative of the ion velocity is bigger at the X point for the realistic mass ratio and the electron densities are different near the O point) the large scale behavior in the two simulations looks similar.

[15] There are some differences in the electron dynamics in the simulations. First, in Figure 5, the electron out-of-plane current is compared for the two mass ratios. The current sheet near the X point is thinner in the case with larger mass ratio. This result is consistent with the findings by *Shay et al.* [2001]. Moreover, in both cases, the large electron current at the O point reduces the total current. The electron current is enhanced by the periodic boundary conditions applied to $x = \pm L_x/2$, as simulations performed with open boundary conditions confirm [*Pritchett*, 2001b].

[16] Second, in Figure 6 the $x$-component of the electron velocity is plotted. It is obvious that the peak velocity is much higher at $m_i/m_e = 1836$ and the peak-to-peak distance is smaller.

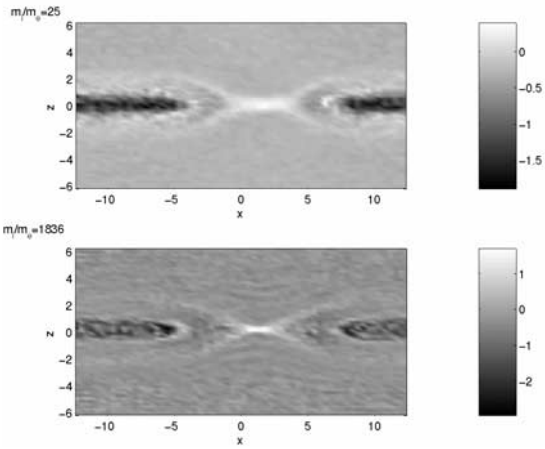


**Figure 5.** Out-of-plane electron current density (normalized to $en_0V_A$) at $\omega_{ci}t = 15$ for $m_i/m_e = 25$ (top) and $m_i/m_e = 1836$ (bottom).

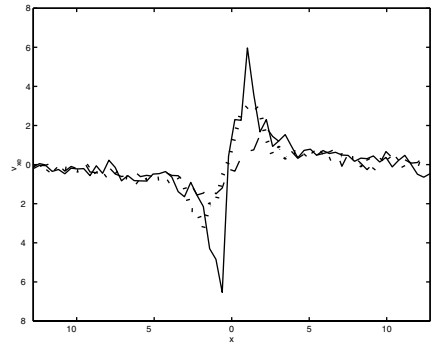

**Figure 6.** $x$-component of the electron velocity, $v_{xe}$, normalized to $V_A$, at $\omega_{ci}t = 15$, $z = 0$, and for $m_i/m_e = 25$ (dashed line), $m_i/m_e = 180$ (dotted line), and $m_i/m_e = 1836$ (solid line).

[17] Assuming that the main contribution to the reconnection field comes from the nongyrotropic electron pressure, scaling laws for the dimensions of the diffusion region ($d_x$, $d_z$), for the peak velocities ($\Delta v_x$, $\Delta v_z$) and for the velocity derivatives ($\partial v_x/\partial x$, $\partial v_z/\partial z$) at the X point, have been deduced both for ions and electrons, and are summarized in Table 1 [*Laval et al.*, 1966; *Hesse et al.*, 1999; *Kuznetsova et al.*, 2000]. We remark that the assumption of a different dissipation mechanism (i.e., electron inertia) leads to different scaling laws [*Burkhart et al.*, 1990] whose predictions agree less well with the simulation results. The scaling laws for $d_{ex}$, $d_{ix}$, $\partial v_{ex}/\partial x$, and $\partial v_{ix}/\partial x$ are discussed using the simulation data plotted in Figures 4 and 6.

[18] The width of the electron diffusion region, $d_{xe}$, is evaluated for $m_i/m_e = 25$ by measuring the peak-to-peak distance in Figure 5, and is $d_{xe} \approx 5\ c/\omega_{pi}$. The peak velocity is $\Delta v_{xe} \approx 1.8\ V_A$. For $m_i/m_e = 180$, the peak-to-peak distance is $d_{xe} \approx 3.2\ c/\omega_{pi}$ and $\Delta v_{xe} \approx 3.1\ V_A$ while, for $m_i/m_e = 1836$, it is $d_{xe} \approx 1.7\ c/\omega_{pi}$ and $\Delta v_{xe} \approx 6.2\ V_A$.

[19] The scaling laws in Table 1 match the simulation results for the three mass ratios.

[20] Since the electron temperature and the $B_z$ field are similar in the three simulations (see Figure 4a for the cases $m_i/m_e = 25$ and $m_i/m_e = 1836$), the scaling law in Table 1 leads to the following theoretical ratio

$$\frac{d_{xe}(m_i/m_e = 25)}{d_{xe}(m_i/m_e = 1836)} \approx 2.92 \tag{3}$$

which is in close agreement with the simulation results, as the measured ratio is ≈2.8. The electron inertia scaling law gives for this ratio a theoretical value of ≈4.19. For the simulations with $m_i/m_e = 25$ and $m_i/m_e = 180$, the measured ratio is ≈1.52, the theoretical ratio based on Table 1 is ≈1.64, while the electron inertia would predict incorrectly ≈1.93.

**Table 1.** Scaling Laws for the Dimensions of the Diffusion Region and the Velocity Derivatives.

| Species | $d_{x,z}$ | $\Delta v_{x,z}$ | $\lvert\frac{\partial v_x}{\partial x}\rvert$, $\lvert\frac{\partial v_z}{\partial z}\rvert$ |
|---|---|---|---|
| electrons | $\left(\frac{m_e T_e}{e^2 B_{z,x}^2}\right)^{1/4}$ | $\left(\frac{e^2 E_{y,rec}^4}{4 m_e T_e B_{z,x}^2}\right)^{1/4}$ | $\frac{eE_{y,rec}}{\sqrt{2 m_e T_e}}$ |
| ions | $\left(\frac{m_i T_i}{e^2 B_{z,x}^2}\right)^{1/4}$ | $\left(\frac{e^2 E_{y,rec}^4}{4 m_i T_i B_{z,x}^2}\right)^{1/4}$ | $\frac{eE_{y,rec}}{\sqrt{2 m_i T_i}}$ |

[21] In the following, we present the detailed comparison between the extreme mass ratios, $m_i/m_e = 25$ and $m_i/m_e = 1836$. Assuming a constant reconnection rate (i.e., a constant $E_{y,rec}$), from Table 1 it is found that the derivative $\partial v_{ex}/\partial x$ scales as $1/\sqrt{m_e}$. The simulations give for $m_i/m_e = 25$, $\partial v_x/\partial x \approx 0.72\ \omega_{ci}$ and for $m_i/m_e = 1836$, $\partial v_x/\partial x \approx 7.28\ \omega_{ci}$. The ratio of these two derivatives (≈10) is similar to the theoretical value (≈8.6) found from Table 1. The small discrepancy may be explained by the higher reconnection rate shown in the case $m_i/m_e = 1836$.

[22] The ion velocity and the dimension of the ion diffusion region should not be influenced by the electron mass according the scaling laws of Table 1 as $E_{y,rec}$ and $B_z$ are almost independent of the electron mass. This is confirmed by Figure 4c. We remark that the slightly greater value of $\partial v_{ix}/\partial x$ in the case $m_i/m_e = 1836$ can be explained again by the slightly greater reconnection rate observed for the physical mass ratio.

[23] From Figure 4, the peak to peak distance for the ion velocity can be measured (for both mass ratios) as $d_{ix} \approx 12.7\ c/\omega_{pi}$. This value can be compared with the theoretical ratio between $d_{ex}$ and $d_{ix}$ obtained from Table 1, which should scale with $[(m_eT_e)/(m_iT_i)]^{1/4}$. The theoretical values of the ratio (≈0.30 for $m_i/m_e = 25$ and ≈0.10 for $m_i/m_e = 1836$) are in good agreement with the simulation results (≈0.39 for $m_i/m_e = 25$ and ≈0.13 for $m_i/m_e = 1836$). The discrepancy can be explained by considering the effect of the periodic boundary conditions applied to $x = \pm L_x/2$ and the resulting injection of ions from the boundary. We remark that the ions are more affected than the electrons because of the larger ion scale and that simulations performed in an open system lead to a larger value for $d_{ix}$ [*Pritchett*, 2001b].

[24] Regarding the ratio between $\partial v_{ex}/\partial x$ and $\partial v_{ix}/\partial x$, which should scale as $[(m_iT_i)/(m_eT_e)]^{1/2}$, the theoretical values from Table 1 (≈11.2 for $m_i/m_e = 25$ and ≈95.8 for $m_i/m_e = 1836$) are in good agreement with the simulation results (≈8.0 for $m_i/m_e = 25$ and ≈81.4 for $m_i/m_e = 1836$). The small discrepancy again may be caused by the reduced $d_{ix}$ because of the periodic boundary conditions.

[25] We conclude that the mass ratio has a minor impact on the reconnection rate, consistent with previous studies, and that it does not affect the larger scale phenomena, such as the ion behavior. However, the mass ratio has a major effect on the electron dissipation region, which appears to rearrange itself in order to maintain the same large scale evolution.

[26] The simulation results agree better with scaling laws based on the hypothesis of magnetic reconnection via non-gyrotropic electron pressure, within the limits imposed by the periodic boundary conditions than with scaling laws based on electron inertia as a dissipation mechanism.

[27] **Acknowledgments.** This research is supported by the United States Department of Energy, under Contract No. W-7405-ENG-36 and by NASA, under the ''Sun Earth Connection Theory Program''. The supercomputer used in this investigation was provided by funding from the JPL Institutional Computing and Information Services and the NASA Offices of Space Science and Earth Science.

## References

Birn, J., et al., Geospace Environment Modelling (GEM) magnetic reconnection challenge, *J. Geophys. Res.*, *106*, 3715, 2001.

Brackbill, J. U., D. W. Forslund, K. B. Quest, and D. Winske, Nonlinear evolution of the lower-hybrid drift instability, *Phys. Fluids*, *27*, 2682, 1984.

Brackbill, J. U. and D. W. Forslund, Simulation of low frequency, electromagnetic phenomena in plasmas, in *Multiple Time Scales*, J. U. Brackbill and B. I. Cohen Eds., Accademic Press, Orlando, pp. 271–310, 1985.

Burkhart, G. R., J. F. Drake, and J. Chen, Magnetic reconnection in collisionless plasma: Prescribed fields, *J. Geophys. Res.*, *95*, 18,833, 1990.

Forslund, D. W., and J. U. Brackbill, Magnetic-field induced surface transport on laser-irradiated foils, *Phys. Rev. Lett.*, *48*, 1614, 1982.

Hesse, M., K. Shindler, J. Birn, and M. Kuznetsova, The diffusion region in collisionless magnetic reconnection, *Phys. Plasmas*, *5*, 1781, 1999.

Hesse, M., J. Birn, and M. M. Kuznetsova, Collisionless magnetic reconnection: electron processes and transport modeling, *J. Geophys. Res.*, *106*, 3721, 2001.

Kuznetsova, M. M., M. Hesse, and D. Winske, Toward a transport model of collisionless magnetic reconnection, *J. Geophys. Res.*, *105*, 7601, 2000.

Kuznetsova, M. M., M. Hesse, and D. Winske, Collisionless reconnection supported by nongyrotropic pressure effects in hybrid and particle simulations, *J. Geophys. Res.*, *106*, 3799, 2001.

Lapenta, G., and J. U. Brackbill, Contact discontinuities in collisionless plasmas: a comparison of hybrid and kinetic simulation, *Geophys. Res. Lett.*, *23*, 1713, 1996.

Laval, G., R. Pellat, and M. Vullemin, Instabilities de plasmas sans collisions, in *Plasma Physics and Controlled Nuclear Fusion Research*, vol. 2, pp. 259–263, Int. Atomic Energy Agency, Vienna, 1966.

Oieroset, M., T. D. Phan, M. Fujimoto, R. P. Lin, and R. P. Lepping, In situ detection of collisionless reconnection in the Earth's Magnetotail, *Nature*, *412*, 414, 2001.

Pritchett, P. L., Particle-in-cell simulations of magnetosphere electrodynamics, *IEEE Trans. Plasma Sci.*, *28*, 1976, 2000.

Pritchett, P. L., Geospace Environment Modelling magnetic reconnection challenge: Simulation with a full particle electromagnetic code, *J. Geophys. Res.*, *106*, 3783, 2001a.

Pritchett, P. L., Collisionless magnetic reconnection in a three dimensional open system, *J. Geophys. Res.*, *106*, 25961, 2001b.

Ricci, P., G. Lapenta, and J. U. Brackbill, A simplified implicit Maxwell solver, *Journal of Computational Physics*, 2002, in press.

Shay, M. A., J. F. Drake, B. N. Rogers, and R. E. Delton, Alvfenic collisionless magnetic reconnection and the Hall term, *J. Geophys. Res.*, *106*, 3759, 2001.

Vu, H. X., and J. U. Brackbill, CELEST1D: An implicit, fully kinetic model for low-frequency Electromagnetic plasma simulation, *Comput. Phys. Commun.*, *69*, 253, 1992.

Vu, H. X., and J. U. Brackbill, Electron kinetic effects in switch-off slow shocks, *J. Geophys. Res.*, *20*, 2015, 1993.

G. Lapenta and J. U. Brackbill, Los Alamos National Laboratory, Los Alamos, NM 87545, USA. (lapenta@lanl.gov; jub@lanl.gov)

P. Ricci, Dipartimento di Energetica, Politecnico di Torino, Corso Duca degli Abruzzi, 24 - 10129 Torino, Italy.